Neutron-deuteron analyzing power data at $E_n = 22.5$ MeV

G. J. Weisel,[*] W. Tornow, A. S. Crowell, J. H. Esterline, G. M. Hale,[†] C. R. Howell, P. D. O'Malley,[‡] J. R. Tompkins,[§] and H. Witała[‖]

Department of Physics, Duke University, Durham, North Carolina 27708, USA
and Triangle Universities Nuclear Laboratory, Durham, North Carolina 27708, USA

(Received 7 February 2014; revised manuscript received 3 April 2014; published 12 May 2014)

We present measurements of n-d analyzing power, $A_y(\theta)$, at $E_n = 22.5$ MeV. The experiment uses a shielded neutron source which produced polarized neutrons via the ^{2}H($\vec{d}$,$\vec{n}$)^{3}He reaction. It also uses a deuterated liquid-scintillator center detector and six pairs of liquid-scintillator neutron side detectors. Elastic neutron scattering events are identified by using time-of-flight techniques and by setting a window in the center detector pulse-height spectrum. The beam polarization is monitored by using a high-pressure helium gas cell and an additional pair of liquid-scintillator side detectors. The n-d $A_y(\theta)$ data were corrected for finite-geometry and multiple-scattering effects using a Monte Carlo simulation of the experiment. The 22.5-MeV data demonstrate that the three-nucleon analyzing power puzzle also exists at this energy. They show a significant discrepancy with predictions of high-precision nucleon-nucleon potentials alone or combined with Tucscon-Melbourne or Urbana IX three-nucleon forces, as well as currently available effective-field theory based potentials of next-to-next-to-next-to-leading order.

DOI: 10.1103/PhysRevC.89.054001 PACS number(s): 25.10.+s, 24.70.+s, 25.40.Dn

I. INTRODUCTION

Over the past two decades, there has been significant progress in the theoretical description of three-nucleon ($3N$) systems. Rigorous $3N$ calculations for bound and scattering states performed using the Faddeev formulation have been accomplished with nucleon-nucleon (NN) potential models, covering Nijmegen, AV18, and CD-Bonn [1–3] alone or combined with standard $3N$ forces such as Tucson-Melbourne (TM99) [4] or Urbana IX (UIX) [5]. With the advance of chiral effective field theory it became possible to construct two- and many-body interactions [6–9] and to apply consistent NN and $3N$ forces ($3N$F) in $3N$ calculations.

Numerous experiments performed for neutron-deuteron and proton-deuteron systems with polarized beams revealed that, at low energies, data for the analyzing power, $A_y(\theta)$, for n-d and p-d systems are significantly higher in magnitude than the predictions of $3N$ Faddeev calculations based on realistic, high-precision NN potentials, even when they are combined with standard $3N$ forces such as TM99 or UIX [10]. This discrepancy is part of what has been named the "$3N$ analyzing power puzzle" ($3N$APP).

A useful way to gauge the $3N$APP is the relative difference (*RD*) defined as the difference between the experimental data and the theoretical values divided by the experimental data at the extrema of $A_y(\theta)$ [11]. A decade ago, the $3N$APP had been well established for n-d scattering at neutron energies from 1.2 to 16 MeV. In Ref. [12] it was pointed out that the energy trend of the *RD* for n-d scattering in the range $E_n = 1.2$ to 10 MeV was different from that for p-d scattering. Simultaneously, it was suggested that this difference in behavior was attributable to the neglect of the Mott-Schwinger interaction between the magnetic momenta of the incoming nucleon and deuteron in three-body calculations. Indeed, theoretical calculations soon confirmed that suggestion, putting the *RD* for both n-d and p-d scattering at about 25% for all energies up to 16 MeV [13,14].

Theoretical investigations revealed that the low energy N-d $A_y(\theta)$ arises predominantly from the interference between the ^3P_j NN force components ($^3P_0$, $^3P_1$, and $^3P_2$) and is highly sensitive to their variation [15]. This suggested that the $3N$APP might be linked to insufficient knowledge of the experimental NN phase shifts in these partial waves and, thereby, incorrect ^3P_j NN force components. Although this option has been pursued, it has proven difficult to modify the ^3P_j phase shifts such that they fit all of the existing $2N$ and $3N$ data [16].

Another possibility is the action of $3N$Fs. When standard $3N$Fs, such as UIX or TM99, are included in three-body calculations, the effects on $A_y(\theta)$ are insufficient to explain the data [17]. However, this does not rule out the possibility. Inconsistency between realistic NN interactions and these standard $3N$Fs is a serious drawback. This problem is cured in the chiral perturbation theory approach, in which NN interactions and $3N$Fs are derived in a consistent way. Therefore, there is hope that the application of chiral forces will help solve the $3N$APP.

The n-d $A_y(\theta)$ data at $E_n = 30$ MeV of Ref. [18] show that there is still a $3N$APP at this energy but that the *RD* is significantly diminished to ≈13%. The lack of n-d $A_y(\theta)$ data between 16 and 30 MeV motivated us to perform

[*]Permanent address: Department of Physics, Penn State Altoona, Altoona, PA 16601.
[†]Permanent address: T-2 Nuclear and Particle Physics, Astrophysics and Cosmology Group, Theoretical Division, Los Alamos National Laboratory, Los Alamos, NM 87545.
[‡]Present address: Department of Physics, University of Notre Dame, Notre Dame, IN 46556.
[§]Present address: National Superconducting Cyclotron Laboratory, Michigan State University, East Lansing, MI 48824.
[‖]Permanent address: Institute of Physics, Jagiellonian University, PL-30059 Cracow, Poland.

measurements in this region, to better characterize the energy dependence of the $3N$APP and to provide data to aid the theoretical development of NN and $3N$ potential models. Our measurement of n-d $A_y(\theta)$ at $E_n = 19.0$ MeV confirmed the existence of the $3N$APP at that energy, with an *RD* in the vicinity of 25% [19]. In the present work, we confirm the $3N$APP at 22.5 MeV, and compare our results to other data, including data for p-d $A_y(\theta)$ at 22.7 MeV [20].

II. EXPERIMENT

Because much of the experimental information for the present $E_n = 22.5$ MeV measurement (for example, all of the detector dimensions) are the same as in our earlier 19-MeV measurement [19], we give a shortened treatment here, one that concentrates on the differences between the two. Polarized deuterons were produced by Triangle Universities Nuclear Laboratory's Atomic Beam Polarized Ion Source (ABPIS), accelerated through an FN-tandem accelerator, and deflected by 20° to the target room. The target room features a shielded neutron source, using a thick wall made of concrete, paraffin, iron, copper, and lead. Originally, we hoped to use a suitable tritiated target and the ^{3}H($\vec{d}$,$\vec{n}$)^{4}He neutron source reaction to start our study in the vicinity of $E_n = 26$ MeV. Unfortunately, it was impossible to secure a tritiated target owing to safety restrictions. Therefore, we retained the deuterium gas cell used in our 19-MeV measurement. The gas cell was filled to a pressure of 7.8 atm and polarized neutrons were produced via the ^{2}H($\vec{d}$,$\vec{n}$)^{3}He source reaction at 0°. The distance from the center of the gas cell to the front face of the thick wall was 180 cm. The deuteron polarized beam current reaching the gas cell was typically 900 nA and the energy spread was ±0.26 MeV. Unfortunately, because the accelerator could not always be brought reliably to the terminal voltage necessary (about 10 MV) for the $E_n = 22.5$ MeV measurement, we did not collect as many angle measurements as originally planned.

The center detector (CD) target was a deuterated liquid scintillator, equivalent to NE232. The center of the CD was located 312 cm downstream from the center of the deuterium gas cell and was surrounded by six pairs of neutron side detectors (filled with NE213 liquid scintillator); the center of each was 150 cm from the center of the CD. The six angles of the $A_y(\theta)$ distribution were chosen to ensure adequate spacing between the side detectors so that rescattering was minimized. The neutron source was encased by the thick wall, having only one exit, to form a well-defined neutron beam. Therefore, the photomultiplier tubes of the CD, the polarimeter gas cell, and the neutron side detectors were shielded from the direct flux of the source.

To cancel instrumental asymmetries, the ABPIS flips the deuteron spin orientation between up and down (in relation to the scattering plane) at a rate of 10 Hz. The measured analyzing power is defined as

$$A_y(\theta) = \frac{1}{P_n}\epsilon(\theta). \quad (1)$$

The quantity $\epsilon(\theta) = \frac{\alpha-1}{\alpha+1}$ is the asymmetry between the left and right detectors, where $\alpha = \sqrt{\frac{L_U R_D}{R_U L_D}}$ for the angle of interest. The R_U and R_D designate the yields for the right detector when the spin is oriented up and down, respectively (and similarly with L_U and L_D for the left detector). The beam polarization, P_n, was monitored with a polarimeter constructed of an active gas cell filled to 100 atm with a mixture of 95% ^{4}He gas and 5% xenon gas and two neutron side detectors. The centers of the side detectors were 40 cm away from the center of the gas cell. The polarimeter was located 70 cm upstream from the CD (242 cm downstream from the source reaction). The polarimeter's side detectors were mounted at an angle of $\theta_{\rm lab} = 112°$, at which the $n + {}^4$He analyzing power is large valued and well determined. In special tests, we used the polarimeter to double-check our beam energy of $E_n = 22.5$ MeV. The $n + {}^4$He system has a sharp resonance at 22.16 MeV [21]. By lowering the accelerator terminal voltage, run to run, and monitoring the polarimeter's asymmetry, we observed the resonance at the expected energy.

Each n-d elastic scattering event was triggered by a timing coincidence between the CD and a particular side detector. For each event, three signals were utilized: the pulse height in the CD, the time of flight (TOF) between the CD and the side detector, and the side-detector signal. The threshold on the constant fraction device for the CD was kept as high as possible to lower the computer dead time but not so high as to cut into the signals associated with the smallest-angle side detector. The thresholds of the side detectors varied from $E_n = 4$ MeV at the forward angle to $E_n = 0.5$ MeV at the back angle and were set by using the electron-recoil edge of a ^{137}Cs source (corresponding, for NE213, to a neutron energy of about 2 MeV).

Pulse-shape discrimination (PSD) made use of a charge-integrating analog-to-digital converter (QDC); one time window integrated the charge in the entire detector pulse and the another integrated the charge in the leading edge. For each detector, a 2D histogram displayed charge in the entire pulse versus charge in the tail only. Applying a 2D gate drawn around the desired elastic events eliminated the events owing to γ rays and reduced the accidental background in the TOF spectra.

Two gates in the TOF spectra were used to create center detector pulse-height (CDPH) spectra. One cut was placed around the elastic counts at approximately 25% of the peak height. A second cut was placed on the lower-time side of the γ-ray peak to determine the number of accidental counts (random coincidences). We made the width of the accidental window greater than that of the elastic window to improve the statistical sample. Separate CDPH spectra were sorted according to whether the right or left detector was involved for spin-up or spin-down events and for elastic or accidental events (a total of eight spectra for each angle pair). The accidental-gated CDPH spectra were then normalized and subtracted from the corresponding elastic-gated spectra.

After accidental subtraction, there was still a small background on the left side of the CDPH's elastic peak. A sample CDPH spectrum is displayed in Fig. 1 for $\theta_{\rm c.m.} = 135.8°$, where the n-d differential cross section is at a minimum. We estimated the background by using two windows to the right and left of the elastic peak (blue vertical lines) and joining them by a line (dashed slanted line). In the following discussion, we refer to this estimate of the background as the "fit background."

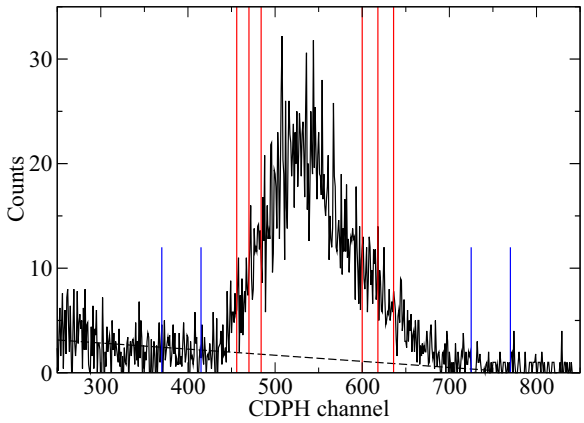

FIG. 1. (Color online) CDPH spectrum corresponding to the neutron side detector at $\theta_{\text{c.m.}} = 135.8^{\circ}$, after the subtraction of the accidental background. The red vertical lines are the three yield gates at 10%, 30%, and 50% of the CDPH peak. The blue vertical lines are the windows used to define the linear fit background, which is shown as the dashed slanted line. These data were collected in 3 days of beam time.

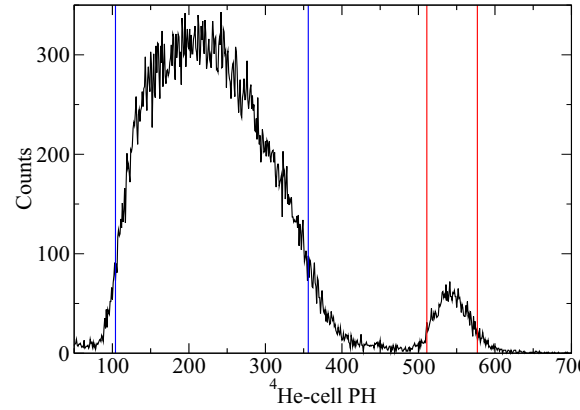

FIG. 2. (Color online) Pulse-height spectrum for the ^{4}He cell. The gate on the right (red vertical lines) was used for the yields of the "elastic neutrons," while the gate on the left (blue vertical lines) was used for the "breakup neutrons." These data were collected in one day of beam time.

The red vertical lines in Fig. 1 are the three gates used for the final yields, placed at approximately 10%, 30%, and 50% of the peak height. In determining the final yields, the 10%, 30%, and 50% yield windows all produced $A_y(\theta)$ results that were consistent with each other, within experimental uncertainties. We judged the 30% window to give a good balance between maximizing yields and reducing background. Separate tests using gate scans, in which a narrow yield gate is stepped across the CDPH spectra, confirmed this choice.

To measure the neutron polarization, P_n, we established detector yields using a method similar to the one just described for n-d scattering. Pulse-shape discrimination gates were determined for the neutron side detectors and in turn were used to filter the TOF spectra. Gates were then set on the elastic peaks in the TOF spectra and used to filter the pulse height of the ^{4}He cell. The resulting pulse-height spectra clearly delineated the peak owing to the "elastic neutrons" (the neutrons originating from the source reaction and scattered elastically from ^{4}He), as can be seen in Fig. 2. During 1 day of our experiment (out of a total of 8 days) we experienced difficulty with the polarimeter resolution, causing the lower-energy "breakup neutrons" (owing to breakup reactions in the deuterium gas cell) to blur into the elastic peak. For this portion of the data, we monitored the large breakup-neutron peak and relied on 2 other days of data using the same beam tuning to calculate the ratio of the asymmetry of the elastic neutrons to that of the breakup neutrons. The ratio was found to be 0.844 ± 0.043. We confirmed that the analyzing power results were consistent, within uncertainties, if we combined all three portions using the same beam tuning or if we left out the portion with poor polarimeter resolution.

The value for polarization of the beam was found by using Eq. (1) along with an effective n-^{4}He analyzing power. A Monte Carlo simulation modeled single scattering from ^{4}He as well as all relevant double-scattering processes involving helium, xenon, iron, and glass. Consideration of finite geometry and double scattering reduced the value taken from an R-matrix analysis from 0.855 to an effective value of 0.833 ± 0.027. The associated uncertainty includes a 3% scale uncertainty of the R-matrix calculation. The P_n was typically about 0.52.

III. ANALYSIS OF THE FIT BACKGROUND

Part of the fit background is attributable to multiple scattering in the target. We determined the magnitude and the asymmetry of the multiple-scattering background by using a Monte Carlo simulation, which included three types of neutron double-scattering events: d-d, d-^{12}C, and ^{12}C-d. The simulation established the ratio of the double counts to total counts, R_{ms}, and the analyzing power, A_{y_ms}, for all three double-scattering processes combined. We also used the simulation to determine the contribution of "edge-effect deuterons" (recoil deuterons that hit the edge of the CD before depositing their full energy in the scintillator), which appear as a flat shoulder on the left side of the elastic peak. The simulation computed the ratio of the edge-effect counts to total counts, R_{ee}, and the analyzing power, A_{y_ee}.

Note that R_{ms}, R_{ee}, and all of the ratios discussed below, were adjusted to the total number of experimental counts (owing to all scattering processes). Note also that all of the ratio values quoted below are based on the 30% CDPH yield window.

Starting from the experimental yields and analyzing powers after accidental subtraction (the stage represented by Fig. 1), we removed multiple-scattering and edge-effect events from the fit background, to leave a "residual background." We used four relations to accomplish this. The first is based on the experimental analyzing power of the accidental-subtracted data, A_{y_asub},

$$R_{\text{asub}}\, A_{y\_\text{asub}} = R_{\text{el}}\, A_{y\_\text{el}} + R_{\text{ms}}\, A_{y\_\text{ms}} + R_{\text{ee}}\, A_{y\_\text{ee}} + R_{\text{res}}\, A_{y\_\text{res}}. \quad (2)$$

The R's are the ratios for each scattering process (relative to total experimental counts), where the subscripts asub, el, ms, ee, and res stand for accidental-subtracted, elastic, multiple-scattering, edge-effect, and residual-background, respectively. The second relation states that all components in the yield gate must add to $R_{\rm asub}$,

$$R_{\rm asub} = R_{\rm el} + R_{\rm ms} + R_{\rm ee} + R_{\rm res}. \quad (3)$$

Depending on the angle and the electronics settings, $R_{\rm asub}$ varied from about 99.5% to 96%. Therefore, the percentage of accidental counts ranged from 0.5% to 4%. The quantities $R_{\rm ms}$, $A_{y\_{\rm ms}}$, $R_{\rm ee}$, and $A_{y\_{\rm ee}}$ (and associated uncertainties) were computed with the Monte Carlo simulation. The ratio $R_{\rm ms}$ varied from 1.6% at $\theta_{\rm c.m.} = 57.4^\circ$ to 7.6% at $\theta_{\rm c.m.} = 151.4^\circ$, while $R_{\rm ee}$ ranged from 0.2% to 0.7% across the same angles.

The third relation is based on the experimental analyzing power of the fit background, $A_{y\_{\rm fit}}$,

$$R_{\rm fit}\, A_{y\_{\rm fit}} = R_{\rm msfit}\, A_{y\_{\rm ms}} + R_{\rm ee}\, A_{y\_{\rm ee}} + R_{\rm res}\, A_{y\_{\rm res}}, \quad (4)$$

where fit refers to the fit background. The fourth relation states that all of the components of the fit background must add to $R_{\rm fit}$,

$$R_{\rm fit} = R_{\rm msfit} + R_{\rm ee} + R_{\rm res}. \quad (5)$$

The ratio $R_{\rm fit}$ ranged from about 3% to 10%. The quantity $R_{\rm msfit}$ appearing in Eqs. (4) and (5) is different from $R_{\rm ms}$ appearing in Eqs. (2) and (3). This is because the shape of the double-scattering background in the CDPH spectra varies; at forward angles, it is nearly flat, while at backward angles, it has a pronounced peak inside the yield gate. The $R_{\rm ms}$ is determined by finding the ratio of simulated doubles to total counts inside the yield gate. The $R_{\rm msfit}$ is found by using the background windows to draw a new linear background resting on the left shoulder of the total double-scattering spectrum; the number of counts of this new background is found and then its ratio is taken with the total experimental counts. The $R_{\rm msfit}$ varied from 1.6% at $\theta_{\rm c.m.} = 57.4^\circ$ to 0.8% at $\theta_{\rm c.m.} = 151.4^\circ$.

Equations (2), (3), (4), and (5) allowed us to solve for the four unknowns $R_{\rm res}$, $R_{\rm el}$, $A_{y\_{\rm res}}$, and $A_{y\_{\rm el}}$. Our determination of the linear fit background and subtraction of multiple-scattering and edge-effect counts led to a reliable determination of $R_{\rm res}$, the ratio of the residual-background counts to total counts, which ranged from about 0.5% to 7%. The ratio of elastic events to total counts, $R_{\rm el}$, was as low as about 80% and as high as 96%.

The analyzing power of the residual background, $A_{y\_{\rm res}}$, is difficult to determine reliably in a low-counting experiment such as this one. We did three different calculations of the final analyzing power values, $A_{y\_{\rm el}}$, for three different treatments of $A_{y\_{\rm res}}$. In the first, we allowed the residual background to be polarized, allowing $A_{y\_{\rm res}}$ to be whatever the above equations gave. In the second calculation we assumed that the residual background had an analyzing power of zero ($A_{y\_{\rm res}} = 0$). In the third, we assumed that the residual background had the same analyzing power as that of the elastic peak ($A_{y\_{\rm res}} = A_{y\_{\rm el}}$).

For three reasons, it is reasonable to assume that $A_{y\_{\rm res}}$ is between zero and that of the elastic counts. First, none of the three calculation methods named in the previous paragraph made significant differences to the final $A_{y\_{\rm el}}$ values beyond experimental uncertainties. Second, one of the most important components of the residual background is attributable to the breakup neutrons, which tail in from the low-energy side of the elastic peak of Fig. 1. From our experience with the polarimeter, we know that the breakup events have an asymmetry that is close to that of the elastic counts. Third, we performed gate scans from the low-energy left shoulder (which carries most of the background) to the high-energy shoulder (which has very few counts). We found that the nominal asymmetry of the left shoulder did not deviate significantly from the range between zero and that of the elastic counts.

In light of these three considerations, we defined the final n-d $A_y(\theta)$ results as the average between the $A_{y\_{\rm el}}$ result using the unpolarized residual background and the $A_{y\_{\rm el}}$ result using the residual background with the same polarization as the elastic counts. As an estimate of the uncertainty associated with this treatment, we took half of the difference between the two analyzing power results. We then added this linearly to the uncertainties of the final $A_y(\theta)$ data.

The library of the Monte Carlo simulation includes n-d $A_y(\theta)$ at 22.5 MeV. Initially, we placed our raw experimental data into the database to perform the first calculations. We then did a self-consistency check by placing the corrected n-d $A_y(\theta)$ data into the library and rerunning the simulation. The analyzing power values for multiple-scattering and edge effects changed only slightly and introduced even smaller changes to the final $A_y(\theta)$ data (well within experimental uncertainties).

IV. RESULTS AND CONCLUSIONS

The final data for n-d $A_y(\theta)$ at $E_n = 22.5$ MeV are displayed in Table I. The statistical uncertainties of the new data are about twice as large as those for our data at 19.0 MeV [19]. The data are also displayed in Figs. 3, 4, and 5, along with an associated Legendre polynomial fit (black dash-dotted curves). Figure 3 compares our data to the range of results (red band) obtained from three-body Faddeev calculations using four realistic, high-precision NN potentials: AV18, CD-Bonn, Nijmegen1, and Nijmegen2. The prediction of the CD-Bonn NN potential lies at the outer edge of the red band and is shown as a black dotted curve. For details of the theoretical formalism and numerical performance, we refer to Refs. [22,23]. The small width of that band reflects nearly on-shell equivalence

TABLE I. Present n-d analyzing power data at $E_n = 22.5$ MeV.

$\theta_{\rm c.m.}$ (deg.)	$A_y(\theta) \pm \Delta A_y(\theta)$
57.4	0.0480 ± 0.0050
85.8	-0.0425 ± 0.0056
110.8	-0.1351 ± 0.0110
124.1	-0.0131 ± 0.0160
135.8	0.2261 ± 0.0214
151.4	0.1064 ± 0.0116

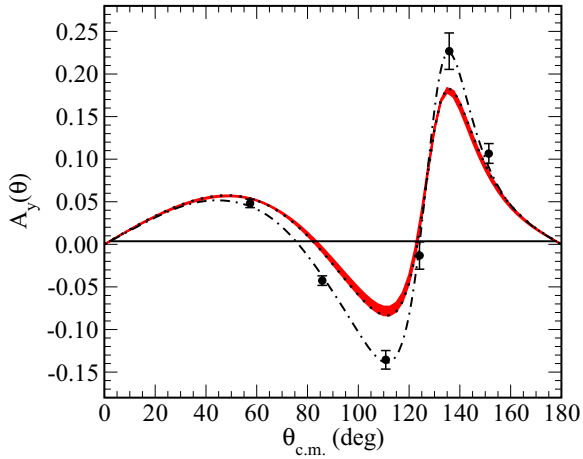

FIG. 3. (Color online) The present n-d analyzing power data at 22.5 MeV (black dots), with an associated Legendre polynomial fit (black dash-dotted curve), compared to the results of Faddeev calculations using different NN potential models. The red band shows the range of results using AV18, CD-Bonn, Nijmegen1, and Nijmegen2. The black dotted curve is the Faddeev prediction based on the CD-Bonn potential.

of these potentials and their high-precision description of experimental NN phase shifts.

Our data differ notably from Faddeev calculations based on NN potentials alone. The discrepancies between the theoretical predictions and the data are especially notable at the minimum of $A_y(\theta)$ at c.m. angles around 110° and at the maximum at c.m. angles around 140°. We follow Ref. [11] and calculate the $RD_{min+max}$ above 16 MeV using the predictions of the AV18 potential. In what follows, we refer to $RD_{min+max}$ simply as RD. The present data give

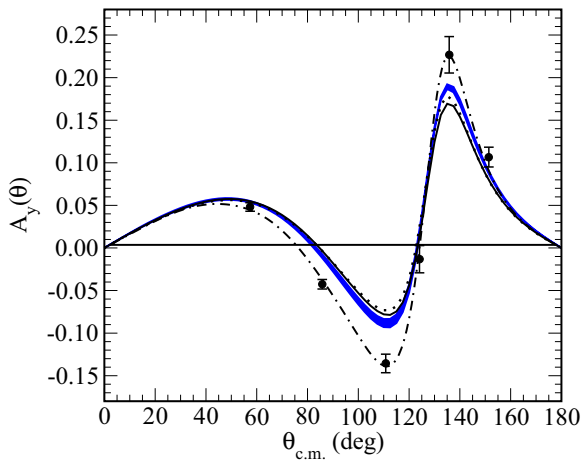

FIG. 4. (Color online) The present n-d analyzing power data at 22.5 MeV (black dots), with an associated Legendre polynomial fit (black dash-dotted curve), compared to results of Faddeev calculations when different NN potentials are combined with 3NFs. The prediction obtained when using AV18 combined with the UIX 3NF is given by the black solid curve, while the prediction of the AV18 NN potential alone is shown by the black dotted curve. The blue band shows the range of results when AV18, CD-Bonn, Nijmegen1, and Nijmegen2 are combined with the TM99 3NF.

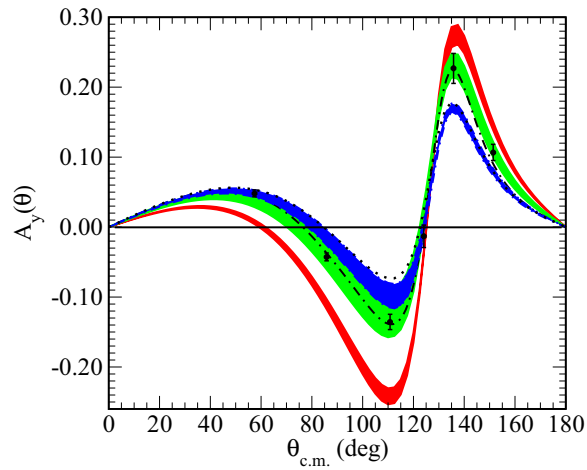

FIG. 5. (Color online) The present n-d analyzing power data at 22.5 MeV (black dots), along with a polynomial fit (black dash-dotted curve), compared to predictions of Faddeev calculations based on five different sets of cutoff parameters [7,8] of chiral NN potentials, in NLO (red band), N^{2}LO (green band), and N^{3}LO (blue band) of the chiral expansion. The prediction using only the AV18 NN potential is shown by the black dotted curve.

a RD of 31% ± 7%, thus confirming the 3NAPP for n-d elastic scattering at $E_n = 22.5$ MeV. Our result is consistent with the discrepancy for $A_y(\theta)$ found in p-d scattering. Comparing the p-d $A_y(\theta)$ at $E_p = 22.7$ MeV of Ref. [20] to a rigorous three-body calculation, Ref. [11] finds an RD of 25% ± 1%.

It is worth pointing out that the RD for the present 22.5-MeV data was already large before we applied the corrections of the previous section. When an associated Legendre polynomial fit is done to our data back at the stage when only accidental counts were subtracted, A_{y_asub} in Eq. (2), we find an RD of 28% ± 7%.

The data reviewed in Ref. [11] suggest that the RD for p-d $A_y(\theta)$ is approximately constant at 25% up to $E_p = 22.7$ MeV, but reduces to 15% at $E_p = 30$ MeV. The n-d $A_y(\theta)$ data now available suggest a similar conclusion for the n-d system. The 19-MeV n-d data of Ref. [19] give an RD of 26% ± 3% (using the AV18 potential). The present 22.5-MeV data give 31% ± 7%, suggesting that the RD does not decrease up to at least $E_n = 22.5$ MeV. Meanwhile, the 30-MeV n-d data of Ref. [18] show a significantly lower RD, of about 13%. We conclude that both p-d and n-d $A_y(\theta)$ follow a closely similar trend for the discrepancy between data and theory.

At low incident neutron energies the standard 3NF models TM99 or UIX are not able to explain the discrepancy between theory and data for $A_y(\theta)$. At 22.5 MeV, it appears unlikely that TM99 or UIX can cure the 3NAPP. Figure 4 shows our data compared to results of 3N Faddeev calculations when the four NN potentials referred to above are combined with standard 3NFs. The black dotted curve is a prediction based on the AV18 potential only, while the black solid curve results when AV18 is combined with the UIX 3NF [5]. The effect of adding this 3NF is practically negligible with exception of the maximum and minimum of $A_y(\theta)$, where it slightly

decreases the AV18 prediction. The UIX $3N$F in combination with AV18 reproduces the triton binding energy. The blue band in Fig. 4 results when the TM99 $3N$F [4] is added to the CD-Bonn, AV18, Nijmegen1, and Nijmegen2 NN potentials. Here, the cutoff parameter is adjusted individually to reproduce the binding energy of ^{3}H. The resulting predictions for $A_y(\theta)$ form the narrow blue band. Clearly, the TM99 $3N$F effects are too small to explain the discrepancy with the data.

As mentioned in Sec. I, with the advance of chiral effective field theory and the construction of NN and $3N$Fs, it was hoped that, in higher orders of chiral expansion, consistent two- and three-body interactions would help to explain the analyzing power puzzle. $3N$Fs first appear in the order next-to-next-to-leading order (N^{2}LO) of chiral expansion [7]. In that order, it is possible for the first time to remove the inconsistency between NN and $3N$Fs in $3N$ Faddeev calculations [24].

Figure 5 shows that, for $E_n = 22.5$ MeV, if the chiral forces are used instead of the standard NN interactions, then the predictions for $A_y(\theta)$ vary with the order of the chiral expansion. Predictions based on the chiral next-to-leading order (NLO) NN interactions (red band) clearly overestimate the $A_y(\theta)$ data, while N^{2}LO chiral potentials (green band) provide quite a good description [25]. When next-to-next-to-next-to-leading order (N^{3}LO) NN chiral forces are used (blue band), the picture resembles that of the standard NN potentials, and a clear discrepancy between data and theory in the region of $A_y(\theta)$ minimum and maximum appears again [25]. Such a behavior can be traced back to the fact that only at the N^{3}LO of the chiral expansion are the experimental NN ^3P_j phases, especially $^3P_2$-$^3F_2$, properly reproduced. Therefore, to answer the question whether consistent chiral NN and $3N$Fs provide the explanation of the $3N$APP, one needs to go to at least the N^{3}LO of the chiral expansion. The first calculations with N^{3}LO $3N$F components [26,27] were recently performed at low energies [25,28]. They clearly show that the $3N$APP cannot be explained using this approach. However, because the 2π-contact term and the $1/m$ relativistic corrections were not yet included in these pioneering calculations, a definitive answer is only possible once the full N^{3}LO $3N$F is included, although the 2π-contact term is not expected to play any significant role at the low energies considered here. In addition, one should include the recently derived N^{4}LO $3N$F components [29,30] together with the associated subleading contributions to the $3N$ contact interactions, which enter at that order of the chiral expansion [31].

Because the role of $3N$F effects appears to be less than was surmised some time ago, it is important again to consider ambiguities in portions of the NN interaction associated with the ^3P_j phase shifts. Owing to the extreme sensivity of N-d $A_y(\theta)$ to these phase shifts and the difficulty of fitting all $2N$ and $3N$ data simultaneously, it is unlikely that the problem can be addressed solely through this approach. The current hope is that a combination of $3N$F effects and improvements to our understanding of the NN interaction, which would lead to a slight modification of the low-energy ^3P_j phase shifts, might solve the $3N$APP. It is possible that the scarce amount of low-energy NN data sensitive to these NN force components will not restrict these phase shifts sufficiently well [32]. In any case, any explanation of the $3N$APP must be able to account for a *RD* for both p-d and n-d $A_y(\theta)$ that is approximately constant at 25% up to 22.5 MeV. At some point after this, the *RD* decreases, reaching about 14% at 30 MeV.

ACKNOWLEDGMENTS

The work was supported by the US Department of Energy under Grant No. DE-FG02-97ER41033. It was also partially supported by the Polish National Science Center under Grant No. DEC-2011/01/B/ST2/00578. We thank M. W. Ahmed, B. J. Crowe III, M. R. Kiser, R. S. Pedroni, and I. Slaus for help with the experiments. The numerical calculations have been performed on the supercomputer cluster of the JSC, Jülich, Germany.

[1] V. G. J. Stoks, R. A. M. Klomp, C. P. F. Terheggen, and J. J. de Swart, Phys. Rev. C **49**, 2950 (1994).
[2] R. B. Wiringa, V. G. J. Stoks, and R. Schiavilla, Phys. Rev. C **51**, 38 (1995).
[3] R. Machleidt, Phys. Rev. C **63**, 024001 (2001).
[4] S. A. Coon and H. K. Han, Few Body Syst. **30**, 131 (2001).
[5] B. S. Pudliner, V. R. Pandharipande, J. Carlson, S. C. Pieper, and R. B. Wiringa, Phys. Rev. C **56**, 1720 (1997).
[6] E. Epelbaum, W. Glöckle, and U.-G. Meißner, Nucl. Phys. A **747**, 362 (2005).
[7] E. Epelbaum, Prog. Part. Nucl. Phys. **57**, 654 (2006).
[8] E. Epelbaum, H. W. Hammer, and U. G. Meißner, Rev. Mod. Phys. **81**, 1773 (2009).
[9] R. Machleidt and D. R. Entem, Phys. Rep. **503**, 1 (2011).
[10] H. Witała, D. Hüber, and W. Glöckle, Phys. Rev. C **49**, R14 (1994).
[11] W. Tornow, J. H. Esterline, and G. J. Weisel, J. Phys. G **35**, 125104 (2008).
[12] E. M. Neidel, W. Tornow, D. E. Gonzalez-Trotter, C. R. Howell, A. S. Crowell, R. A. Macri, R. L. Walter, G. J. Weisel, R. S. Pedroni, D. M. Markoff, and H. Witała, Phys. Lett. B **552**, 29 (2003).
[13] H. Witała, J. Golak, R. Skibiński, C. R. Howell, and W. Tornow, Phys. Rev. C **67**, 064002 (2003).
[14] A. Kievsky, M. Viviani, and L. E. Marcucci, Phys. Rev. C **69**, 014002 (2004).
[15] H. Witała and W. Glöckle, Nucl. Phys. A **528**, 48 (1991).
[16] W. Tornow, H. Witała, and A. Kievsky, Phys. Rev. C **57**, 555 (1998).
[17] H. Witała, W. Glöckle, J. Golak, A. Nogga, H. Kamada, R. Skibiński, and J. Kuroś-Zolnierczuk, Phys. Rev. C **63**, 024007 (2001).
[18] H. Dobiasch, R. Fisher, B. Haesner, H. O. Klages, P. Schwarz, B. Zeitnitz, R. Maschuw, K. Sinram, and K. Wick, Phys. Lett. B **76**, 195 (1978).
[19] G. J. Weisel *et al.*, Phys. Rev. C **81**, 024003 (2010).

[20] W. Grüebler, V. König, P. A. Schmelzbach, F. Sperisen, B. Jenny, R. E. White, F. Seiler, and H. W. Roser, Nucl. Phys. A **398**, 445 (1983); F. Sperisen, W. Grüebler, V. König, P. A. Schmelzbach, K. Elsener, B. Jenny, C. Schweizer, J. Ulbricht, and P. Doleschall, *ibid.* **422**, 81 (1984).
[21] B. Hoop, Jr. and H. H. Barschall, Nucl. Phys. **83**, 65 (1966).
[22] W. Glöckle, H. Witała, D. Hüber, H. Kamada, and J. Golak, Phys. Rep. **274**, 107 (1996).
[23] D. Hüber, H. Kamada, H. Witała, and W. Glöckle, Acta Phys. Pol. B **28**, 1677 (1997).
[24] E. Epelbaum, A. Nogga, W. Glöckle, H. Kamada, Ulf-G. Meißner, and H. Witała, Phys. Rev. C **66**, 064001 (2002).
[25] H. Witała, J. Golak, R. Skibiński, and K. Topolnicki, arXiv:1310.0198 [nucl-th].
[26] V. Bernard, E. Epelbaum, H. Krebs, and Ulf-G. Meißner, Phys. Rev. C **77**, 064004 (2008).
[27] V. Bernard, E. Epelbaum, H. Krebs, and Ulf-G. Meißner, Phys. Rev. C **84**, 054001 (2011).
[28] H. Witała, J. Golak, R. Skibiński, K. Topolnicki, H. Kamada, E. Epelbaum, W. Gloeckle, H. Krebs, W. N. Polyzou, and A. Nogga, Few-Body Syst. **54**, 897 (2013).
[29] H. Krebs, A. Gasparyan, and E. Epelbaum, Phys. Rev. C **85**, 054006 (2012).
[30] H. Krebs, A. Gasparyan, and E. Epelbaum, Phys. Rev. C **87**, 054007 (2013).
[31] L. Girlanda, A. Kievsky, and M. Viviani, Phys. Rev. C **84**, 014001 (2011).
[32] T. Tornow and W. Tornow, Few-Body Syst. **26**, 1 (1999).